

AttriReBoost: A Gradient-Free Propagation Optimization Method for Cold Start Mitigation in Attribute Missing Graphs

Mengran Li¹, Chaojun Ding¹, Junzhou Chen¹, Wenbin Xing¹, Cong Ye¹, Ronghui Zhang¹,
Songlin Zhuang², Jia Hu³, Tony Z. Qiu⁴, and Huijun Gao⁵, *Fellow, IEEE*

Abstract—Missing attribute issues are prevalent in the graph learning, leading to biased outcomes in Graph Neural Networks (GNNs). Existing methods that rely on feature propagation are prone to cold start problem, particularly when dealing with attribute resetting and low-degree nodes, which hinder effective propagation and convergence. To address these challenges, we propose *AttriReBoost* (ARB), a novel method that incorporates propagation-based method to mitigate cold start problems in attribute-missing graphs. ARB enhances global feature propagation by redefining initial boundary conditions and strategically integrating virtual edges, thereby improving node connectivity and ensuring more stable and efficient convergence. This method facilitates gradient-free attribute reconstruction with lower computational overhead. The proposed method is theoretically grounded, with its convergence rigorously established. Extensive experiments on several real-world benchmark datasets demonstrate the effectiveness of ARB, achieving an average accuracy improvement of 5.11% over state-of-the-art methods. Additionally, ARB exhibits remarkable computational efficiency, processing a large-scale graph with 2.49 million nodes in just 16 seconds on a single GPU. Our code is available at <https://github.com/limengran98/ARB>.

Index Terms—Attribute-Missing Graphs, Cold Start Problem, Feature Propagation, Graph Learning.

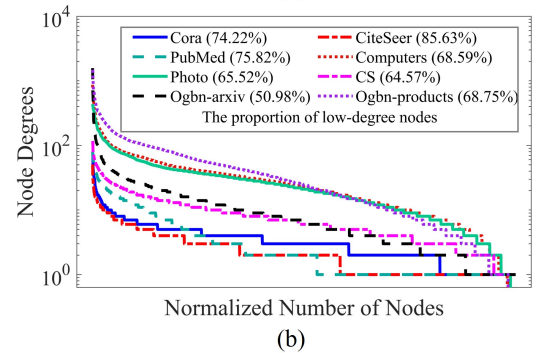
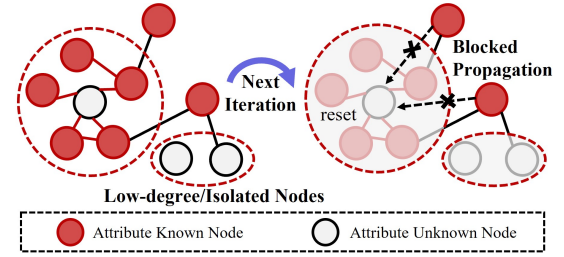


Fig. 1: (a) Cold start examples in attribute-missing graphs. (b) Real-world datasets present a long-tail distribution, and tail/cold start nodes are difficult to participate in propagation.

This work has been submitted to the IEEE for possible publication. Copyright may be transferred without notice, after which this version may no longer be accessible.

This project is jointly supported by the Shenzhen Fundamental Research Program (No. JCYJ20240813151129038), the National Natural Science Foundation of China (Nos. 52172350, 51775565), the Guangdong Basic and Applied Research Foundation (No. 2022B1515120072), the Guangzhou Science and Technology Plan Project (No. 2024B01W0079), the Nansha Key R&D Program (No. 2022ZD014), and the China Postdoctoral Science Foundation (No. 2013T60904). (*Corresponding author: Ronghui Zhang.*)

Mengran Li, Junzhou Chen, Wenbin Xing, Ye Cong, and Ronghui Zhang are with School of Intelligent Systems Engineering, Shenzhen Campus of Sun Yat-sen University, Shenzhen 518107, P.R. China. Ronghui Zhang is also with the School of Transportation Science and Engineering, Harbin Institute of Technology, Harbin 150080, P.R. China (e-mail: limr39@mail2.sysu.edu.cn; chenjunzhou@mail.sysu.edu.cn; xingwb, yecong5@mail2.sysu.edu.cn; zhangrh25@mail.sysu.edu.cn).

Songlin Zhuang is with the Yongjiang Laboratory, Ningbo 315202, P.R. China (e-mail: songlin-zhuang@ylab.ac.cn).

Jia Hu is with the Key Laboratory of Road and Traffic Engineering of the Ministry of Education, Tongji University, Shanghai 201804, P.R. China (e-mail: hujia@tongji.edu.cn).

Tony Z. Qiu is with Department of Civil and Environmental Engineering, University of Alberta, Edmonton, AB T6G 2R3, Canada (e-mail: zhijun-qiu@ualberta.ca).

Huijun Gao is with the Research Institute of Intelligent Control and Systems, Harbin Institute of Technology, Harbin 150080, P.R. China (e-mail: hjgao@hit.edu.cn).

I. INTRODUCTION

The significance of graph data in representing complex networks is well-established [1]–[5], yet most real-world scenarios often suffer from missing attribute features that represent node semantic information in graphs [6]–[9]. Therefore, the task of reconstructing missing attributes in graphs becomes essential for comprehensive network analysis [10], [11]. Recent advancements based Graph Neural Networks (GNNs) [12]–[14] provide opportunities for effective missing attribute reconstruction. However, GNNs typically struggle with oversmoothing and high computational costs [15]. While Feature propagation methods [16], [17] could address these issues, they still face a common challenge: **the cold start problem in reconstructing missing attributes**.

Two key factors contribute to the cold start problem in attribute-missing graphs. First, methods like [16], [17] require resetting known nodes after each feature propagation iteration to preserve initial attributes. However, as shown in Figure 1(a), this resetting causes unknown nodes to repeatedly receive the same initial attributes from known nodes, hindering global information propagation. Second, while high-quality and rich

connectivity can facilitate feature propagation, real-world graphs often contain many low-degree or isolated nodes, leading to a long-tail distribution of node degrees [18], [19]. As illustrated in Figure 1(b), approximately 70% of nodes in each dataset are low-degree, making it difficult for propagation methods to effectively generalize to these tail or cold start nodes, thereby impacting the reconstruction of missing attributes.

Inspired by techniques like Feature Propagation (FP) [16] and Personalized PageRank [20], we propose a novel method named *AttriReBoost* (ARB) to enhance attribute reconstruction and mitigate the cold start problem. ARB improves propagation connectivity by redefining initial boundary conditions and introducing effective virtual edges. By redefining boundary conditions, ARB dynamically transmits attributes from both nearby and distant known nodes to unknown nodes, avoiding information loss from repeated resets and ensuring continuous, updated attribute information. The virtual edges create a virtually fully connected overlay, allowing low-degree or isolated nodes to better participate in the propagation process, ensuring robust connectivity for convergence.

Building on these ideas, we establish an optimization function and derive ARB’s iterative algorithm, rigorously proving its convergence using the *Banach-Fixed Point Theorem*. ARB’s gradient-free propagation eliminates the computational load of backpropagation and gradient learning, introducing only two additional hyperparameters compared to FP [16], thus achieving attribute reconstruction with lower computational cost. Experimental validation shows that ARB outperforms state-of-the-art methods in both feature propagation and node classification. Compared to FP and Stochastic Gradient Descent (SGD) methods [21], ARB achieves faster convergence and early stopping, making it a more efficient choice for large-scale and cold start-sensitive applications.

The innovations of this paper are summarized as follows:

- To address the cold start problem in attribute-missing graphs, ARB introduces innovative techniques that re-define boundary conditions and integrate virtual edges into the feature propagation process. Grounded in both empirical insights and rigorous mathematical theory, these advancements enhance node connectivity and significantly improve propagation efficiency.
- ARB enhances the efficiency of graph-based learning by utilizing a gradient-free message passing framework, which significantly accelerates convergence and enables early stopping. This method simplifies the computational process while enabling more efficient and scalable processing of large-scale graphs.
- Extensive experiments on real-world datasets demonstrate the superiority of ARB over state-of-the-art methods, showing an average accuracy improvement of 5.11%. Additionally, ARB demonstrates significant computational efficiency, processing large-scale graphs with 2.49 million nodes in just 16 seconds on a single GPU, achieving faster and more stable convergence. which is of significant value in real-world applications where computational resources and time are critical.

This paper is structured as follows: Section II provides a review of related work, Section III outlines the problem,

Section IV introduces the proposed methods, Section V presents the experimental results, and Section VI concludes with a discussion of potential future research.

II. RELATED WORK

A. Attribute Missing Graph Learning

In the early work, [22] utilized mean pooling to aggregate the features of neighboring nodes. [23] proposed the Singular Value Thresholding (SVT) algorithm, which completed matrix imputation by adjusting singular values. Besides, incomplete multi-view learning [24]–[27] has been widely studied as it addresses the challenge of missing or incomplete data across multiple views, enabling the development of robust models that can leverage information from different perspectives even when some data is missing or corrupted.

GNN based Methods With the advent of deep learning, [10], [28] used GNNs to generate missing data. [29] and [30] employed attributed random walk techniques to create nodes embedded on bipartite graphs with node attributes. [31] proposed graph denoising autoencoders, where each edge encoded the similarity between patterns to complete missing attributes. [32] transformed missing attributes into Gaussian mixture distribution, enabling Graph Convolutional Networks (GCN) [33] to be applied to incomplete network attributes. SAT [12] and SVGA [13] employed separate subnetworks for nodes attributes and graph structure to impute missing data with structural information, using GANs and Graph Markov Random Fields (GMRFs) [34] respectively, guided by shared latent space assumptions. Amer [35] introduced a unified framework that combines attribute completion and embedding learning, leveraging mutual information maximization and a novel GAN-based attribute-structure relationship constraint to improve performance. ITR proposed by [14] initially filled in missing attributes using the graph’s structural information, then adaptively refined the estimated latent variables by combining observed attributes and structural information. MAGAE [36], on the other hand, employed a regularized graph autoencoder that mitigates spectral concentration issues by maximizing graph spectral entropy, enhancing the imputation of missing attributes. For community detection in attribute-missing networks, CAST [37] adopted a Transformer-based architecture, integrating contrastive learning, sampling, and propagation strategies to effectively capture node relationships and address missing attribute challenges. [38] suggested imputing attributes in the input space by leveraging parameter initialization and graph diffusion to generate multi-view information.

Propagation based Methods In addition to the aforementioned deep learning-based methods, some propagation-based methods have been widely focused on due to their low complexity and high scalability. [16] introduced the FP method, which reconstructed missing features by minimizing Dirichlet energy and diffusing known features across the graph structure. [17] proposed the Pseudo-Confidence Feature Imputation (PCFI) method, which enhanced feature propagation by incorporating a pseudo-confidence-based weighting mechanism during propagation.

B. Cold Start Problem

The cold start problem, which arises in scenarios such as recommendation systems and information pushing, is a significant challenge due to the lack of sufficient user or item data at the initial stages. To mitigate this issue, several approaches have been proposed. For instance, [39] and [40] explored transfer learning methods to leverage knowledge from related tasks or domains, aiming to improve the performance of models with limited data. Additionally, [41] combined multi-task learning for graph pre-training, allowing for the transfer of useful representations across different tasks to enhance the model's ability to generalize from sparse information. Meanwhile, [42] and [43] focused on specialized distillation methods to transfer knowledge from well-trained models to improve the training of models with insufficient data. However, despite the success of these approaches in addressing cold start problems, they do not specifically tackle the issue of attribute-missing graphs, where the challenge lies in recovering missing or incomplete node attributes while maintaining graph structure and learning performance.

C. Summary

Although GNN-based methods generally perform well with attribute-missing graphs, they suffer from high computational complexity and resource demands, limiting their scalability. Additionally, GNNs are prone to the oversmoothing problem, where node representations become indistinguishable as layers increase. In contrast, propagation-based methods are simpler and more scalable but struggle with the cold start problem, as they rely heavily on existing graph structure and known attributes, leading to suboptimal feature reconstruction and difficulty in capturing nuanced relationships.

III. PRELIMINARIES

A. Problem Definition

We define an attribute-missing graph $G = (\mathcal{V}, \mathcal{E}, \mathbf{X}, k)$, where $\mathcal{V} = \mathcal{V}_k \cup \mathcal{V}_u$. \mathcal{V}_k and \mathcal{V}_u denote the sets of nodes with known and unknown (missing) attribute features, respectively. The node attribute matrix is denoted by $\mathbf{X} \in \mathbb{R}^{N \times F}$. For the total nodes N , only nodes k possess attributes. The adjacency matrix is $\mathbf{A} \in \{0, 1\}^{N \times N}$, diagonal degree matrix is \mathbf{D} , symmetric normalized adjacency matrix is $\tilde{\mathbf{A}} = \mathbf{D}^{-1/2} \mathbf{A} \mathbf{D}^{-1/2}$, \tilde{a}_{ij} represent the individual elements of $\tilde{\mathbf{A}}$, and symmetric normalized Laplacian matrix $\mathbf{L} = \mathbf{I} - \tilde{\mathbf{A}}$. The goal of this work is to reconstruct the missing attribute feature and apply it to downstream classification tasks.

B. Feature Propagation

To reconstruct the missing attributes \mathbf{X}_u based on the known attribute features \mathbf{X}_k and the graph G , the optimization function of Feature Propagation (FP) [16] can be expressed as a process of minimizing the Dirichlet energy [44], [45]. For distinction, define the matrix \mathbf{Z} as the initial attribute feature matrix of the

graph, encompassing both known and unknown node attributes. The optimization function can be expressed as:

$$\min_{\mathbf{X}} \mathcal{L} = \sum_{(i,j) \in \mathcal{E}} \tilde{a}_{ij} (\mathbf{x}_i - \mathbf{x}_j)^2 = \text{tr}(\mathbf{X}^\top \mathbf{L} \mathbf{X}) \quad \text{s.t. } \mathbf{X}_k = \mathbf{Z}_k \quad (1)$$

Solving the optimization function yields:

$$\nabla \mathcal{L}(\mathbf{X}) = \mathbf{L} \mathbf{X} = (\mathbf{I} - \tilde{\mathbf{A}}) \mathbf{X} = 0 \quad \text{s.t. } \mathbf{X}_k = \mathbf{Z}_k \quad (2)$$

Initially, we set $\mathbf{X}^{(0)} = \mathbf{Z}$. The number of iterations is defined as l . The attributes are updated by $\tilde{\mathbf{A}}$, and the known nodes are reinitialize after current propagation:

$$\begin{cases} \mathbf{X}^{(l+1)} = \tilde{\mathbf{A}} \mathbf{X}^{(l)} & \triangleright \text{Propagation} \\ \mathbf{X}_k^{(l+1)} = \mathbf{Z}_k & \triangleright \text{Reset} \end{cases} \quad (3)$$

Although traditional feature propagation methods lay a foundation for reconstructing missing features, they struggle to address the cold start problem. Motivated by this, the following section introduces the proposed ARB.

IV. PROPOSED METHOD

A crucial prerequisite for attribute-missing graph learning is the accurate and effective recovery of missing attributes. However, the cold start problem worsen recovery, as low-degree and isolated nodes in the graph can hinder iteration convergence. This paper proposes a novel *AttriReBoost* (ARB) method. To address the cold start problem, ARB boosts propagation based methods, redefines the initial boundary conditions of FP, and establishes virtual edges to enhance node connectivity, reconstructs missing attributes accurately and effectively. The overall framework is illustrated in Figure 2.

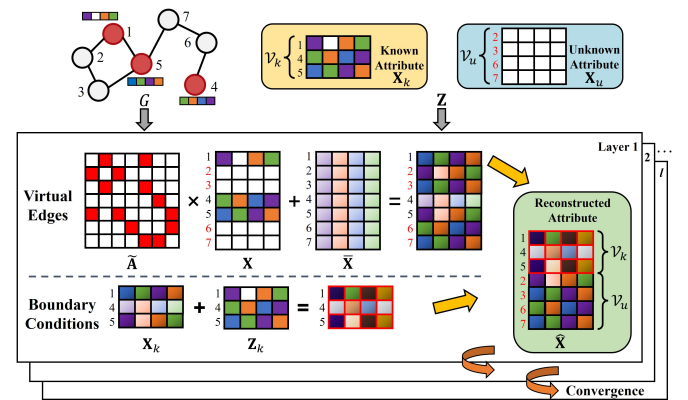


Fig. 2: The overall framework of ARB. ARB address the cold start problem in attribute-missing graph learning by enhancing node connectivity through virtual edges and redefining initial boundary conditions. ARB boosts propagation-based methods to accurately and effectively recover missing attributes.

A. Redefinition of Boundary Conditions

An intuitive method to reconstructing missing attributes is to converge to an optimal value by iterative approximating during propagation. However, the repetitive resetting of known node attributes in propagation disrupts the smooth flow of

information. As shown in Figure I(a), for unknown nodes, they receive same information stems from the initial attributes \mathbf{Z}_k of known nodes during each iteration, if the majority of their neighbors are known nodes, hindering the propagation of global information. To address this, ARB redefines the boundary conditions of the optimization Equation (1) and dynamically adjust the initialization of known nodes.

Statement 1: The New Boundary Conditions term in Equation (4) incorporates known node attributes into the optimization process. This term is expressed in Lagrangian form as a sum of squared differences, weighted by the parameter η .

$$\begin{aligned} \min_{\mathbf{X}} \mathcal{L} &= \underbrace{\sum_{(u,v) \in \mathcal{E}} \tilde{\mathbf{a}}_{uv} (\mathbf{x}_u - \mathbf{x}_v)^2}_{\text{Feature Propagation}} + \underbrace{\eta \sum_{v \in \mathcal{V}_k} (\mathbf{x}_v - \mathbf{z}_v)^2}_{\text{New Boundary Conditions}} \\ &= \text{tr}(\mathbf{X}^\top \mathbf{L} \mathbf{X} + \eta (\mathbf{X}_k - \mathbf{Z}_k)^\top (\mathbf{X}_k - \mathbf{Z}_k)). \end{aligned} \quad (4)$$

B. Virtual Edges for Connectivity

In real-world graphs, many nodes are sparsely connected, and some are even isolated, resulting in a long-tail distribution of node degrees. Consequently, it struggles to effectively generalize to tail or cold start nodes for feature propagation. Observing the iterative Equation (3), $\mathbf{X}_k^{(l+1)} = \tilde{\mathbf{A}} \mathbf{X}^{(l)}$, since $\tilde{\mathbf{A}}$ is a symmetric normalized matrix, its spectral radius is not strictly less than 1, which could not guarantee convergence. To address this issue, a fully connected graph $\bar{G} = (\mathcal{V}, \bar{\mathcal{E}}, \mathbf{Z}, k)$ is introduced, where the virtual edge set $\bar{\mathcal{E}}$ assumes that all node pairs are connected.

Statement 2: Extending the New Boundary Conditions term, the Virtual Edges term in Equation (5) introduces additional connectivity via $\bar{\mathcal{E}}$ to enhance global information. This term is represented as Dirichlet energy, incorporated as a penalty term, weighted by the parameter θ .

$$\begin{aligned} \min_{\mathbf{X}} \mathcal{L} &= \underbrace{\sum_{(u,v) \in \mathcal{E}} \tilde{\mathbf{a}}_{uv} (\mathbf{x}_u - \mathbf{x}_v)^2}_{\text{Feature Propagation}} + \underbrace{\eta \sum_{v \in \mathcal{V}_k} (\mathbf{x}_v - \mathbf{z}_v)^2}_{\text{New Boundary Conditions}} \\ &+ \underbrace{\theta \sum_{(i,j) \in \bar{\mathcal{E}}} \bar{\mathbf{a}}_{ij} (\mathbf{x}_i - \mathbf{x}_j)^2}_{\text{Virtual Edges}} \\ &= \text{tr}(\mathbf{X}^\top \mathbf{L} \mathbf{X} + \eta (\mathbf{X}_k - \mathbf{Z}_k)^\top (\mathbf{X}_k - \mathbf{Z}_k) + \theta \mathbf{X}^\top \mathbf{L}_1 \mathbf{X}), \end{aligned} \quad (5)$$

where $\bar{\mathbf{a}}_{ij}$ is the element of the normalized adjacency matrix of \bar{G} , $\mathbf{L}_1 = \frac{N}{N-1} \mathbf{I} - \frac{1}{N-1} \mathbf{J}$, and \mathbf{J} is an all-ones matrix.

C. Optimization Function of ARB

To optimize the Equation (5), we first define the matrix $\mathbf{I}_k^0 = \text{diag}(\{\lambda_1, \lambda_2, \dots, \lambda_N\})$, $\lambda_i = \begin{cases} 1 & \text{if } i \in \mathcal{V}_k \\ 0 & \text{otherwise} \end{cases}$, representing the known and unknown nodes, and explores the gradient $\nabla \mathcal{L}(\mathbf{X})$:

$$\begin{aligned} \nabla \mathcal{L}(\mathbf{X}) &= \mathbf{L} \mathbf{X} + \eta (\mathbf{X}_k - \mathbf{Z}_k) + \theta \mathbf{L}_1 \mathbf{X} = 0 \\ \Rightarrow (\mathbf{I} + \eta \mathbf{I}_k^0 + \theta \mathbf{I}) \mathbf{X} &= \tilde{\mathbf{A}} \mathbf{X} + \eta \mathbf{I}_k^0 \mathbf{Z} + \theta \left(\frac{N}{N-1} \bar{\mathbf{X}} - \frac{1}{N-1} \mathbf{X} \right) \\ \Rightarrow \left(\frac{\theta N + N - 1}{N-1} \mathbf{I} + \eta \mathbf{I}_k^0 \right) \mathbf{X} &= \tilde{\mathbf{A}} \mathbf{X} + \eta \mathbf{I}_k^0 \mathbf{Z} + \frac{\theta N}{N-1} \bar{\mathbf{X}}, \end{aligned} \quad (6)$$

where $\bar{\mathbf{X}}$ represents the mean of \mathbf{X} . Considering unknown nodes and known nodes separately, Equation (6) is further simplified to:

$$\begin{bmatrix} \mathbf{X}_k \\ \mathbf{X}_u \end{bmatrix} = \begin{bmatrix} \left[\frac{\eta}{\frac{\theta N + N - 1}{N-1} + \eta} \mathbf{Z} + \frac{1}{\frac{\theta N + N - 1}{N-1} + \eta} \tilde{\mathbf{A}} \mathbf{X} + \frac{\frac{\theta N}{N-1}}{\frac{\theta N + N - 1}{N-1} + \eta} \bar{\mathbf{X}} \right]_k \\ \left[\frac{N-1}{\theta N + N - 1} \tilde{\mathbf{A}} \mathbf{X} + \frac{\theta N}{\theta N + N - 1} \bar{\mathbf{X}} \right]_u \end{bmatrix}. \quad (7)$$

Let $\alpha = \frac{N-1}{\theta N + N - 1}$ and $\beta = \frac{1/\alpha}{1/\alpha + \eta}$, both of which belong to the open interval $(0, 1)$, we have:

$$\begin{bmatrix} \mathbf{X}_k \\ \mathbf{X}_u \end{bmatrix} = \begin{bmatrix} [(1-\beta)\mathbf{Z} + \beta(\alpha \tilde{\mathbf{A}} \mathbf{X} + (1-\alpha)\bar{\mathbf{X}})]_k \\ [\alpha \tilde{\mathbf{A}} \mathbf{X} + (1-\alpha)\bar{\mathbf{X}}]_u \end{bmatrix}. \quad (8)$$

We then relate ARB recursively as follows:

$$\begin{cases} \mathbf{X}^{(l+1)} = \alpha \tilde{\mathbf{A}} \mathbf{X}^{(l)} + (1-\alpha) \bar{\mathbf{X}}^{(l)} & \triangleright \text{Global Propagation} \\ \mathbf{X}_k^{(l+1)} = \beta \mathbf{X}_k^{(l)} + (1-\beta) \mathbf{Z}_k & \triangleright \text{Moving Reset} \end{cases} \quad (9)$$

ARB process is shown in Algorithm 1.

Algorithm 1 AttriReBoost

Require: known attribute matrix \mathbf{Z}_k , normalized adjacency matrix $\tilde{\mathbf{A}}$, hyperparameters α , β and l

- 1: $\mathbf{X} \leftarrow 0, \mathbf{X}_k \leftarrow \mathbf{Z}_k$
- 2: **for** l iterations **do**
- 3: $\mathbf{X} \leftarrow \alpha \tilde{\mathbf{A}} \mathbf{X} + (1-\alpha) \bar{\mathbf{X}}$ \triangleright Global Propagation
- 4: $\mathbf{X}_k \leftarrow \beta \mathbf{X}_k + (1-\beta) \mathbf{Z}_k$ \triangleright Moving Reset
- 5: **end for**
- 6: **Until** \mathbf{X} convergence

Ensure: Reconstructed attributes $\hat{\mathbf{X}}_u$

D. ARB Convergence and Steady State Proof

The ultimate goal is to demonstrate that the proposed ARB can iteratively approach the optimal value to achieve attribute reconstruction. By introducing metric space, the convergence of the proposed ARB has been rigorously proven at the theoretical level.

\square *Convergence Proof:* Since $\tilde{\mathbf{A}}$ be the symmetric normalized adjacency matrix, $\rho(\tilde{\mathbf{A}}) \leq 1$ [46]. Let $\mathbf{B} = \alpha \tilde{\mathbf{A}} + (1-\alpha) \frac{1}{N} \mathbf{J}$ is a strong connection matrix (irreducible matrix), $\rho(\mathbf{B}) = \|\mathbf{B}\|_2 \leq \alpha \|\tilde{\mathbf{A}}\|_2 + (1-\alpha) \|\mathbf{J}\|_2 = \alpha \rho(\tilde{\mathbf{A}}) + (1-\alpha) \rho(\mathbf{J}) \leq 1$. Equation (9) can be written as:

$$\begin{bmatrix} \mathbf{X}_k \\ \mathbf{X}_u \end{bmatrix} = \begin{bmatrix} \beta \mathbf{B}_{kk} & \beta \mathbf{B}_{ku} \\ \mathbf{B}_{uk} & \mathbf{B}_{uu} \end{bmatrix} \begin{bmatrix} \mathbf{X}_k \\ \mathbf{X}_u \end{bmatrix} + \begin{bmatrix} (1-\beta) \mathbf{Z}_k \\ 0 \end{bmatrix}. \quad (10)$$

Let $\mathbf{K} = \begin{bmatrix} \beta \mathbf{B}_{kk} & \beta \mathbf{B}_{ku} \\ \mathbf{B}_{uk} & \mathbf{B}_{uu} \end{bmatrix}$, $\mathbf{C} = \begin{bmatrix} (1-\beta) \mathbf{Z}_k \\ 0 \end{bmatrix}$, $0 \leq \mathbf{K} \leq \mathbf{B}$ elementwise. Because $\beta < 1$, which means $\mathbf{K} \neq \mathbf{B}$, therefore $0 \leq \mathbf{K} < \mathbf{B}$.

Given that \mathbf{B} is a strongly connected matrix, and $\mathbf{K} \geq 0$, $\mathbf{B} \geq 0$, $\mathbf{K} + \mathbf{B}$ is also a strongly connected matrix and therefore irreducible. And with $0 \leq \mathbf{K} \leq \mathbf{B}$ elementwise and $\mathbf{K} \neq \mathbf{B}$, we can deduce that $\rho(\mathbf{K}) < \rho(\mathbf{B})$. Therefore $\rho(\mathbf{K}) < \rho(\mathbf{B}) \leq 1$, that is, $\rho(\mathbf{K}) < 1$.

Additionally, if \mathbf{B} can be expressed as a diagonal matrix composed of a series of strongly connected matrices \mathbf{B}_i . Responsive, \mathbf{K} can also be decomposed into a series of $0 \leq \mathbf{K}_i \leq \mathbf{B}_i$ elementwise, and there exists at least one \mathbf{K}_j that satisfies $\mathbf{K}_j \neq \mathbf{B}_j$, so $\rho(\mathbf{K}_j) < 1$, and

$$\rho(\mathbf{K}) = \max \frac{\mathbf{X}^\top \mathbf{K} \mathbf{X}}{\mathbf{X}^\top \mathbf{X}} = \max \frac{\sum \mathbf{x}_i^\top \mathbf{K}_i \mathbf{x}_i}{\sum \mathbf{x}_i^\top \mathbf{x}_i} < \max \frac{\sum \mathbf{x}_i^\top \mathbf{x}_i}{\sum \mathbf{x}_i^\top \mathbf{x}_i} = 1. \quad (11)$$

According Equation (10), Let $f(\mathbf{X}) = \mathbf{K}\mathbf{X} + \mathbf{C}$. Take the spectral norm $\|\mathbf{X}\|_2 = \sqrt{\rho(\mathbf{X}^\top \mathbf{X})}$ as the measure. From $\rho(\mathbf{K}) < 1$, we know $\rho(\mathbf{K}^\top \mathbf{K}) < 1$. And use the feature vector $\{\mathbf{v}_1, \mathbf{v}_2, \dots, \mathbf{v}_n\}$ of $\mathbf{K}^\top \mathbf{K}$ to represent $\Delta \mathbf{X} = \sum_i w_i \mathbf{v}_i$, where w_i are the coefficients. Then:

$$\begin{aligned} \|\Delta f(\mathbf{X})\|_2 &= \|\mathbf{K}\Delta \mathbf{X}\|_2 = \Delta \mathbf{X}^\top \mathbf{K}^\top \mathbf{K} \Delta \mathbf{X} \\ &= \sum_{ij} w_i w_j \mathbf{v}_i^\top \lambda_j \mathbf{v}_j \leq \rho(\mathbf{K}^\top \mathbf{K}) \sum_{ij} w_i w_j \mathbf{v}_i^\top \mathbf{v}_j \\ &= \rho(\mathbf{K}^\top \mathbf{K}) \Delta \mathbf{X}^\top \Delta \mathbf{X} = \rho(\mathbf{K}^\top \mathbf{K}) \|\Delta \mathbf{X}\|_2 < \|\Delta \mathbf{X}\|_2. \end{aligned} \quad (12)$$

That is, f is a contraction mapping, and according to *Banach Fixed Point Theorem* [47], $\mathbf{X} = f(\mathbf{X})$ has a unique fixed-point. Therefore, the recursive expression $\mathbf{X}^{(l+1)} = \mathbf{K}\mathbf{X}^{(l)} + \mathbf{C}$ converges to a unique value. ■

□ *Steady State Proof:* According to Equations (5) and (6), the steady state of ARB can be given as follows:

$$\begin{aligned} \nabla \mathcal{L}(\mathbf{X}) &= \mathbf{L}\mathbf{X} + \eta(\mathbf{X}_k - \mathbf{Z}_k) + \theta \mathbf{L}_1 \mathbf{X} = 0 \\ \implies (\mathbf{L} + \eta \mathbf{I}_k^0 + \theta \mathbf{L}_1) \mathbf{X} &= \eta \mathbf{Z}_k \\ \implies \mathbf{X} &= (\mathbf{L} + \eta \mathbf{I}_k^0 + \theta \mathbf{L}_1)^{-1} \eta \mathbf{Z}_k \end{aligned} \quad (13)$$

Consider the Rayleigh quotient:

$$\begin{aligned} \mathbf{R} &= \frac{\mathbf{X}^\top (\mathbf{L} + \eta \mathbf{I}_k^0 + \theta \mathbf{L}_1) \mathbf{X}}{\mathbf{X}^\top \mathbf{X}} \\ &= \frac{\sum_{(i,j) \in \mathcal{E}} \bar{\mathbf{a}}_{ij} (\mathbf{x}_i - \mathbf{x}_j)^2 + \eta \sum_{i \in \mathcal{V}_k} \mathbf{x}_i^2 + \sum_{(i,j) \in \bar{\mathcal{E}}} \bar{\mathbf{a}}_{ij} (\mathbf{x}_i - \mathbf{x}_j)^2}{\sum_{i \in \mathcal{V}} \mathbf{x}_i^2} > 0. \end{aligned} \quad (14)$$

In fact, $\mathbf{X}^\top (\mathbf{L} + \eta \mathbf{I}_k^0 + \theta \mathbf{L}_1) \mathbf{X} = 0 \iff \forall i, j \in \mathcal{V}$, s.t. $\mathbf{X}_i = \mathbf{X}_j = 0$, but $\mathbf{X} \neq 0$. Thus, all eigenvalues of $\mathbf{L} + \eta \mathbf{I}_k^0 + \theta \mathbf{L}_1$ are positive, making the matrix invertible. ■

E. Complexity, Scalability, and Learning

The goal of ARB is to reconstruct missing attributes. Compared to FP, it introduces only two additional adjustable hyperparameters, α and β , thereby retaining all the advantages of FP in terms of low complexity $O(|\mathcal{E}| + F|\mathcal{V}|)$ and scalability [16]. ARB is a gradient-free method that can be run as preprocessing on the CPU for large graphs and integrated with any graph learning model, like GCN [33] and GAT [48], to generate predictions for downstream tasks [49].

V. EXPERIMENTATION AND ANALYSIS

To thoroughly verify ARB's effectiveness in attribute reconstruction and downstream tasks, we address the following key questions:

- Q1:** How does ARB perform in attribute reconstruction?
- Q2:** How does ARB perform in downstream tasks after attribute-missing reconstruction?
- Q3:** How does ARB address the cold start problem and convergence issues?
- Q4:** Are all components of ARB effective?
- Q5:** How does ARB perform under different missing rates?
- Q6:** How is the computational efficiency of ARB?

TABLE I: Data statistics.

Dataset	Type	Nodes	Edges	Feature	Classes	Subgraphs
Cora	Binary	2,708	5,278	1,433	7	78
CiteSeer	Binary	3,327	4,228	3,703	6	438
Computers	Binary	13,752	245,861	767	10	314
Photo	Binary	7,650	119,081	745	8	136
PubMed	Continuous	19,717	44,324	500	3	1
CS	Continuous	18,333	81,894	6,805	15	1
Oggn-Arxiv	Continuous	169,343	1,166,243	128	40	1
Oggn-Products	Continuous	2,449,029	61,859,140	100	47	1

A. Experimental Setup

1) *Dataset:* We chose eight public graph datasets included Cora, CiteSeer, PubMed [50], CS [51], Computers, Photo [51], and large-scale datasets Oggn-Arxiv and Oggn-Products [52] for this study, each containing vital information like nodes, edges and attribute features. Table I shows data statistics for each dataset.

2) *Baseline:* We compare ARB with several baseline methods. NeighAgg [22] aggregates features of one-hop neighbors using mean pooling. GNN* refers to the best-performing models among GCN [33], GraphSAGE [53], and GAT [48]. GraphRNA [29] and ARWMF [30] are recent feature generation methods. SAT [12] uses a shared latent space for features and graph structure. Amer [35] integrates attribute completion and embedding learning using GAN-based constraints. SVGA [13] employs Gaussian Markov random fields for feature estimation. ITR [14] fills missing attributes using graph structure and refines them iteratively. FP [16] uses Dirichlet energy minimization to impute features. PCFI [17] introduces pseudo-confidence for feature imputation. MAGAE [36] mitigates spectral concentration via a graph autoencoder. CAST [37] is a Transformer-based method combining contrastive learning and propagation. MATE [38] enhances attribute imputation through graph diffusion and multi-view information.

3) *Implementation Details:* Unless otherwise stated, we allocate 40% of the observable data as the training set and consider 60% of the attribute-missing nodes as target nodes. We split target nodes into validation and test sets in a 1:5 ratio, consistent with previous work [13], [14]. ARB performs missing attribute reconstruction according to the process outlined in Algorithm 1, executing l iterations. In each iteration, the neighborhood information of each node is first gathered through 3rd line in Algorithm 1, filling in the missing features, during which known features are also updated.

TABLE II: Evaluation of ARB and baseline methods on binary features for attribute reconstruction. Best results are indicated in **blue**, second best results are **green**.

Metric	Method	Venue	Cora			CiteSeer			Computers			Photo		
			@10	@20	@50	@10	@20	@50	@10	@20	@50	@10	@20	@50
Recall	NeighAgg	/	0.0906	0.1413	0.1961	0.0511	0.0908	0.1501	0.0321	0.0593	0.1306	0.0329	0.0616	0.1361
	GNN*	/	0.1350	0.1812	0.2972	0.0620	0.1097	0.2058	0.0273	0.0533	0.1278	0.0295	0.0573	0.1324
	GraphRNA	KDD'19	0.1395	0.2043	0.3142	0.0777	0.1272	0.2271	0.0386	0.0690	0.1465	0.0390	0.0703	0.1508
	ARWMF	NeurIPS'19	0.1291	0.1813	0.2960	0.0552	0.1015	0.1952	0.0280	0.0544	0.1289	0.0294	0.0568	0.1327
	SAT	TPAMI'22	0.1653	0.2345	0.3612	0.0811	0.1349	0.2431	0.0421	0.0746	0.1577	0.0427	0.0765	0.1635
	Amer	TCYB'22	0.1584	0.2220	0.3368	0.0814	0.1333	0.2248	0.0425	0.0739	0.1523	0.0435	0.0772	0.1617
	SVGA	KDD'22	0.1718	0.2486	0.3814	0.0943	0.1539	0.2782	0.0437	0.0769	0.1602	0.0446	0.0798	0.1670
	ITR	IJCAI'22	0.1656	0.2372	0.3652	0.0972	0.1552	0.2679	0.0446	0.0780	0.1530	0.0434	0.0778	0.1635
	FP	LOG'22	0.1620	0.2268	0.3406	0.0850	0.1380	0.2311	0.0425	0.0741	0.1544	0.0434	0.0773	0.1627
	PCFI	ICLR'23	0.1609	0.2261	0.3434	0.0812	0.1342	0.2294	0.0429	0.0750	0.1547	0.0436	0.0774	0.1618
	MEGAE	AAAI'23	0.1730	0.2355	0.3660	0.0958	0.1497	0.2619	0.0431	0.0748	0.1543	0.0433	0.0768	0.1610
	CAST	TCSS'24	0.1720	0.2475	0.3703	0.0949	0.1506	0.2577	0.0427	0.0749	0.1558	0.0438	0.0774	0.1623
	MATE	IF'24	0.1731	0.2460	0.3768	0.1000	0.1589	0.2716	0.0447	0.0782	0.1618	0.0442	0.0795	0.1649
	ARB	Ours	0.1856	0.2599	0.3851	0.1046	0.1643	0.2823	0.0449	0.0784	0.1627	0.0455	0.0804	0.1681
nDCG	NeighAgg	/	0.1217	0.1548	0.1850	0.0823	0.1155	0.1560	0.0788	0.1156	0.1923	0.0813	0.1196	0.1998
	GNN*	/	0.1791	0.2099	0.2711	0.1026	0.1423	0.2049	0.0673	0.1028	0.1830	0.0712	0.1083	0.1896
	GraphRNA	KDD'19	0.1934	0.2362	0.2938	0.1291	0.1703	0.2358	0.0931	0.1333	0.2155	0.0959	0.1377	0.2232
	ARWMF	NeurIPS'19	0.1824	0.2182	0.2776	0.0859	0.1245	0.1858	0.0694	0.1053	0.1851	0.0727	0.1098	0.1915
	SAT	TPAMI'22	0.2250	0.2723	0.3394	0.1385	0.1834	0.2545	0.1030	0.1463	0.2346	0.1047	0.1498	0.2421
	Amer	TCYB'22	0.2254	0.2690	0.3301	0.1364	0.1817	0.2415	0.1048	0.1468	0.2307	0.1062	0.1513	0.2408
	SVGA	KDD'22	0.2381	0.2894	0.3601	0.1579	0.2076	0.2892	0.1068	0.1509	0.2397	0.1084	0.1549	0.2472
	ITR	IJCAI'22	0.2288	0.2770	0.3448	0.1645	0.2129	0.2870	0.1086	0.1612	0.2415	0.1069	0.1526	0.2440
	FP	LOG'22	0.2306	0.2755	0.3359	0.1427	0.1891	0.2497	0.1063	0.1491	0.2345	0.1066	0.1514	0.2411
	PCFI	ICLR'23	0.2272	0.2723	0.3342	0.1367	0.1829	0.2445	0.1061	0.1487	0.2341	0.1063	0.1511	0.2406
	MEGAE	AAAI'23	0.2440	0.2858	0.3552	0.1611	0.2062	0.2798	0.1063	0.1487	0.2337	0.1063	0.1507	0.2401
	CAST	TCSS'24	0.2401	0.2877	0.3505	0.1606	0.2071	0.2771	0.1044	0.1447	0.2335	0.1062	0.1510	0.2410
	MATE	IF'24	0.2373	0.2861	0.3550	0.1720	0.2212	0.2950	0.1090	0.1535	0.2424	0.1086	0.1553	0.2465
	ARB	Ours	0.2594	0.3043	0.3749	0.1768	0.2267	0.3043	0.1107	0.1553	0.2450	0.1104	0.1565	0.2493

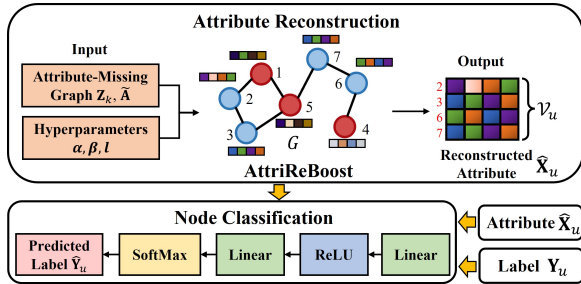


Fig. 3: Specific implementation process of attribute reconstruction and node classification.

Then, in 4th line of Algorithm 1, the known node attributes are reset, allowing them to participate in the next iteration. After completing the iterations, the final output $\hat{\mathbf{X}}_u$, representing the reconstructed missing attributes, is denoted as $\hat{\mathbf{X}}_u$. Both our attribute reconstruction and node classification tasks solely use $\hat{\mathbf{X}}_u$ as input, with no other inputs involved. This method ensures that we assess the usability of the reconstructed features in isolation. For the node classification task, all methods use a two-layer MLP as the classifier, with an Adam optimizer set to a learning rate of 1e-2, a hidden channel dimension of 256, and a maximum training epoch of 1000, performing five-fold cross-validation [16]. The overall implementation process is illustrated in Figure 3.

TABLE III: Evaluation of ARB and baseline methods on continuous features for attribute reconstruction. Best results are **blue**, second best results are **green**.

Method	Venue	PubMed		CS	
		RMSE	CORR	RMSE	CORR
NeighAgg	/	0.0186	-0.2133	0.0952	-0.2279
GNN*	/	0.0168	-0.0010	0.0850	0.0179
GraphRNA	KDD'19	0.0172	-0.0352	0.0897	-0.1052
ARWMF	NeurIPS'19	0.0165	0.0434	0.0827	0.0710
SAT	TPAMI'22	0.0165	0.0378	0.0820	0.0958
Amer	TCYB'22	0.0185	0.0123	0.0826	0.0233
SVGA	KDD'22	0.0166	0.0280	0.0824	0.0740
ITR	IJCAI'22	0.0164	0.0324	0.0832	0.0543
FP	LOG'22	0.0165	0.0778	0.0798	0.1657
PCFI	ICLR'23	0.0166	0.0729	0.0883	0.1571
MAGAE	AAAI'23	0.0185	-0.1010	0.0854	0.1656
CSAT	TCSS'24	0.0165	0.0710	0.0886	0.1101
MATE	IF'24	0.0165	0.0345	0.0832	0.0645
ARB	Ours	0.0161	0.0981	0.0777	0.1811
Method	Venue	Ogbn-Arxiv		Ogbn-Products	
FP	LOG'22	0.1101	0.0028	0.5847	0.1574
PCFI	ICLR'23	0.1101	0.0030	0.5848	0.1574
ARB	Ours	0.1002	0.0170	0.5840	0.1577

B. Attribute Reconstruction Results (Q1)

To evaluate the quality of attribute reconstruction, the similarity probability between the reconstructed attributes and the true attributes at each dimension is the main target. To

TABLE IV: Evaluation of the Accuracy (%) of ARB and baseline methods on node classification. Best results are **blue**, second best results are **green**.

Dataset	SAT	SVGA	ITR	FP	PCFI	ARB
Cora	76.44	78.70	81.43	84.37	84.64	85.78
CiteSeer	60.10	62.33	67.15	66.21	66.83	67.20
PubMed	46.18	62.27	72.36	80.62	80.73	82.21
Computers	74.10	72.56	83.88	83.71	84.02	86.08
Photo	87.62	88.55	90.75	87.41	89.56	91.74
CS	76.72	82.93	85.67	89.30	89.60	91.54
Ogbn-Arxiv	22.44	21.59	24.72	51.50	51.21	52.48
Ogbn-Products	27.61	27.30	28.12	75.01	76.23	81.28
<i>Average</i>	58.90	62.03	66.76	77.27	77.85	79.79

TABLE V: Semi-supervised node classification accuracy (%) at various missing rates. Best results are **blue**.

Dataset	50%			90%		
	FP	PCFI	ARB	FP	PCFI	ARB
Cora	80.71	80.51	81.38	79.09	78.84	80.20
CiteSeer	65.58	68.32	67.55	66.10	66.13	66.77
PubMed	74.87	75.12	75.97	74.28	74.06	75.08
Photo	91.07	90.38	91.43	88.67	88.32	90.01
Computers	83.81	81.76	84.07	81.21	81.12	81.78
<i>Average</i>	79.21	79.22	80.08	77.87	77.69	78.77
Dataset	99%			99.5%		
	FP	PCFI	ARB	FP	PCFI	ARB
Cora	77.73	77.87	78.62	76.81	76.91	77.12
CiteSeer	66.06	65.26	66.61	64.10	65.45	66.90
PubMed	72.09	73.42	73.46	72.12	72.20	72.99
Photo	88.13	87.98	88.44	87.29	87.80	88.09
Computers	79.37	79.75	79.78	78.06	79.51	79.05
<i>Average</i>	76.68	76.85	77.38	75.67	76.37	76.83

achieve this, we follow the experimental setup of [13], using Recall@k and nDCG@k as metrics to assess binary feature datasets with k set to {10, 20, 50}. For continuous feature datasets, we use RMSE and CORR as metrics. The results of the attribute reconstruction are summarized in Tables II and III. Our method consistently outperforms the baseline method, with an average improvement of **2.87%** and **9.96%** over the second-best method, respectively.

Further analysis of comparison shows that GNN based methods, such as SVGA, ITR and MATE, achieve competitive results on binary feature datasets compared to propagation-based baselines like FP and PCFI. However, in continuous feature datasets, propagation methods demonstrate a stronger advantage. This indicates that feature propagation-based methods have superior capabilities in complex attribute reconstruction. Additionally, since these methods do not provide effective solutions for the cold start problem, their performance remains consistently suboptimal compared to ARB.

Thus, in response to Q1, our conclusion is: **ARB exhibits strong performance in reconstructing features for attribute-missing graphs, effectively recovering missing attributes with high accuracy across various datasets.**

C. Node Classification Results (Q2)

In our node classification experiments, our primary focus is to validate the effectiveness of the reconstructed features for downstream tasks. Therefore, we only use the reconstructed attribute features \hat{X}_u of the unknown nodes \mathcal{V}_u for five-fold cross-validation, a choice influenced by methods like SAT [12] and SVGA [13]. We input the features that achieve the highest Recall@10 and CORR metrics in attribute reconstruction into a linear classifier for five-fold cross validation. The results of the node classification are summarized in Table IV. Our method consistently outperforms the baseline method, with an average improvement of **2.49%** over the second-best method.

Further analysis reveals that while deep generative methods like SAT and SVGA demonstrate certain advantages in attribute reconstruction, they underperform in downstream node classification tasks, particularly on continuous feature datasets. Notably, a key advantage of propagation-based methods like FP and PCFI is their independence from gradient descent, enabling efficient training on CPU [16]. This eliminates the need for memory-intensive graph partitioning and batch processing, providing a natural advantage on large-scale datasets like Ogbn-Arxiv and Ogbn-Products. Moreover, ARB outperforms other propagation-based algorithms, demonstrating its strong reconstructed attributes in downstream tasks.

However, we note that the experimental setup differs from those used in FP [16] and PCFI [17], where semi-supervised node classification includes all nodes \mathcal{V} with known attributes. Additionally, these methods follow the standard dataset splits and settings from PyG¹ and OGBN² and achieve competitive results even under extreme missing rates (99% and 99.5%). To ensure a fair comparison and to assess ARB’s effectiveness in semi-supervised node classification, we conducted additional experiments under these conditions. As shown in Table V, ARB outperforms other methods, demonstrating superior performance across both regular and extreme missing conditions.

Thus, in response to Q2, our conclusion is: **ARB demonstrates strong adaptability in downstream tasks after attribute reconstruction, outperforming baseline methods, particularly in large-scale datasets.**

D. Convergence Speed to Verify Cold Start (Q3)

Judging ARB’s performance in mitigating the cold start problem could be done by evaluating its early stopping and convergence speed capabilities.

As shown in Figure 4(a), in weakly connected graphs like Cora, ARB reaches the optimal solution in fewer epochs (Epoch ≈ 10), demonstrating faster attribute reconstruction. Similarly, in strongly connected graphs like PubMed (Figure 4(b)), ARB adapts and approaches the optimal solution by Epoch ≈ 15 , highlighting its efficiency in resolving the cold start problem with minimal training.

During the iterative process, ARB converges faster than deep generative methods. As shown in Figure 4(c), it outperforms SVGA and FP in both convergence speed and reconstruction

¹<https://pyg.org/>

²<https://ogb.stanford.edu/docs/nodeprop/>

TABLE VI: Evaluation of ARB and baseline methods on binary features for attribute reconstruction. Best results are indicated in **blue**. NA means not available.

Metric	Method	Node Type	Cora			CiteSeer			Computers			Photo		
			@10	@20	@50	@10	@20	@50	@10	@20	@50	@10	@20	@50
Recall	w/o BC&VE	isolated	NA	NA	NA	0.0000	0.0052	0.0151	0.0120	0.0259	0.0609	0.0125	0.0285	0.0653
	ARB	isolated	NA	NA	NA	0.0457	0.0916	0.1701	0.0308	0.0616	0.1441	0.0332	0.0611	0.1390
	w/o BC&VE	low degree	0.1504	0.2075	0.3117	0.0777	0.1286	0.2171	0.0463	0.0802	0.1611	0.0382	0.0696	0.1487
	ARB	low degree	0.1757	0.2475	0.3735	0.0981	0.1569	0.2710	0.0497	0.0841	0.1715	0.0481	0.0855	0.1739
	w/o BC&VE	other	0.1839	0.2482	0.3708	0.1250	0.1870	0.2990	0.0430	0.0750	0.1566	0.0436	0.0775	0.1629
	ARB	other	0.1903	0.2771	0.4055	0.1257	0.1915	0.3175	0.0442	0.0771	0.1604	0.0441	0.0790	0.1657
nDCG	w/o BC&VE	isolated	NA	NA	NA	0.0000	0.0107	0.0108	0.0325	0.0462	0.0795	0.0358	0.0534	0.0895
	ARB	isolated	NA	NA	NA	0.0613	0.1001	0.1525	0.0687	0.1057	0.1848	0.0766	0.1128	0.1934
	w/o BC&VE	low degree	0.2086	0.2457	0.3029	0.1271	0.1708	0.2306	0.1059	0.1469	0.2255	0.0879	0.1272	0.2037
	ARB	low degree	0.2451	0.2928	0.3593	0.1645	0.2135	0.2888	0.1109	0.1529	0.2375	0.1118	0.1581	0.2453
	w/o BC&VE	other	0.2623	0.3061	0.3720	0.2141	0.2674	0.3438	0.1073	0.1506	0.2387	0.1069	0.1516	0.2417
	ARB	other	0.2695	0.3272	0.3968	0.2177	0.2742	0.3592	0.1098	0.1562	0.2460	0.1081	0.1548	0.2497

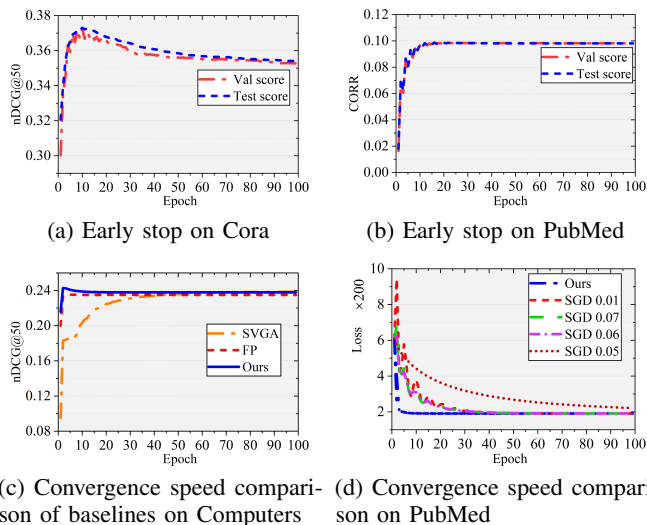


Fig. 4: Training process and convergence speed.

accuracy, achieving satisfactory results early (Epoch=2) and enabling early stopping. This rapid convergence reduces overall computation time, making ARB more efficient for large-scale and time-sensitive applications. Similar to SGD-based methods, ARB initializes unknown node attributes to zero while preserving known ones. However, ARB’s dynamic propagation method significantly outperforms SGD in terms of convergence speed, as shown in Figure 4(d), by adjusting the boundary of known nodes and propagating information without the need for backpropagation.

Furthermore, we conduct a separate evaluation of isolated nodes and low-degree nodes to verify the effectiveness of the ARB method in the attribute reconstruction task. Table VI shows a significant performance improvement when comparing the FP and ARB models, particularly for isolated nodes and low-degree nodes. The proposed ARB method substantially enhances the attribute reconstruction performance for these nodes, effectively addressing the cold-start problem. This further validates the effectiveness and practicality of our

method.

Thus, in response to Q3, our conclusion is: **ARB is able to effectively tackle the cold start problem and convergence difficulty, ensuring more stable and rapid convergence.**

E. Ablation and Hyperparameters Experiments (Q4)

Tables VII and VIII present the results of the ablation study for ARB. In the tables, “w/o BC” denotes the removal of the new boundary condition mechanism in ARB, and “w/o VE” indicates the removal of the virtual edge mechanism in ARB. The results show that ARB always achieves optimal performance across various scenarios, outdoing the other schemes in performance. Further analysis reveals that the new boundary conditions contribute more significantly to performance improvement compared to the virtual edges. While the virtual edge mechanism enhances global connectivity, it inevitably brings some noise. Therefore, to fully leverage its benefits, proper tuning of the parameters α and β is necessary.

The virtual edges and new boundary conditions add a propagation channel but may also introduce noise. To address this, the hyperparameter α regulates their influence weight. Additionally, the number of propagation layers l also impacts the results. Therefore, the three key hyperparameters— α , β , and l —are critical to ARB’s performance and require careful tuning.

Regarding hyperparameter tuning, we propose the Heuristic Hyperparameter Searcher, using nDCG or CORR as the target metric. Starting at $(\alpha, \beta) = (0.5, 0.5)$, neighboring points at distance d are evaluated, and the best-scoring point becomes the new center. The process repeats, halving d when no better points are found, until the stopping condition is met.

Concluded from Figure 5, the optimal result suggests setting α within the range of 0.9 to 1. β is crucial for the redefinition of boundary conditions in ARB, and must be tuned for each specific dataset to achieve optimal performance. At lower l values, the focus is on local neighborhood structures, which is crucial for nodes in small components with limited connectivity. As l increases, global propagation enriches the feature space with structural information from distant parts of the network.

TABLE VII: Ablation experiments for attribute reconstruction. Best results are **blue**.

Metric	Method	Cora			CiteSeer			Computers			Photo		
		@10	@20	@50	@10	@20	@50	@10	@20	@50	@10	@20	@50
Recall	w/o BC	0.1555	0.2199	0.3303	0.0821	0.1339	0.2266	0.0430	0.0750	0.1557	0.0436	0.0773	0.1622
	w/o VE	0.1771	0.2488	0.3693	0.0927	0.1482	0.2470	0.0442	0.0770	0.1595	0.0447	0.0793	0.1655
	ARB	0.1856	0.2599	0.3851	0.1046	0.1643	0.2823	0.0449	0.0784	0.1627	0.0455	0.0804	0.1681
nDCG	w/o BC	0.2195	0.2637	0.3220	0.1373	0.1828	0.2444	0.1060	0.1488	0.2349	0.1064	0.1512	0.2411
	w/o VE	0.2491	0.2968	0.3611	0.1576	0.2059	0.2712	0.1086	0.1522	0.2402	0.1087	0.1544	0.2458
	ARB	0.2594	0.3043	0.3749	0.1768	0.2267	0.3043	0.1107	0.1553	0.2450	0.1104	0.1565	0.2493

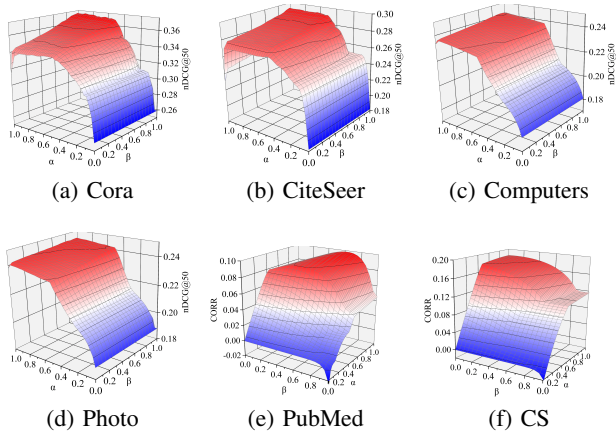
TABLE VIII: Ablation experiments for node classification. Best results are **blue**.

Method	Cora	CiteSeer	PubMed	Computers
w/o BC	84.42	66.89	81.61	84.65
w/o VE	84.86	66.54	82.12	85.83
ARB	85.78	67.20	82.81	86.08

Method	Photo	CS	Ogbn-Arxiv	Ogbn-Products
w/o BC	90.23	90.38	49.91	79.56
w/o VE	90.56	89.57	52.01	80.44
ARB	91.74	91.54	52.48	81.28

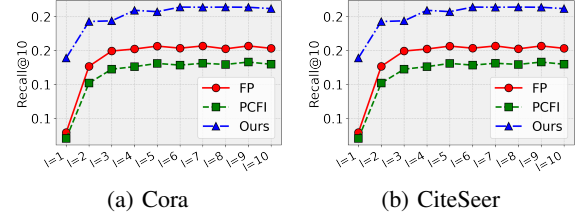
Figure 6 shows that ARB effectively addresses propagation barriers and oversmoothing issues across depths from $l = 1$ to $l = 10$, significantly outperforming algorithms like FP and PCFI. In contrast, SVGA suffers from oversmoothing as l increases, leading to performance degradation, while ARB consistently maintains or improves performance with deeper propagation.

Thus, in response Q4, our conclusion is: **Each component of ARB has been validated and proven effective. Removing any component, including boundary conditions or virtual edges, leads to a drop in performance. The hyperparameters α , β and l need to be adjusted for different datasets to achieve the best results.**

Fig. 5: Hyperparameter value α and β validation.

F. Sensitivity Analysis on Missing Rates (Q5)

We conduct a series of attribute reconstruction experiments to validate the robustness of ARB, with missing attribute rates

Fig. 6: Comparison of different propagation times l .

ranging from 40% to 99%, using Recall@10 as the primary evaluation metric. As shown in Table IX, ARB demonstrates exceptional performance in attribute reconstruction tasks, particularly under high missing rates, confirming its robustness. Additionally, we observe that FP outperforms SVGA and ITR at higher missing rates, further highlighting the robustness of feature propagation-based methods.

Therefore, for Question 5, our conclusion is: **ARB maintains robust performance across different missing rates, even when the missing rate is as high as 99%.**

TABLE IX: Comparison of methods under different missing rates (%). MR stands for missing rate. Best results are **blue**.

Cora	Recall@10					CiteSeer	Recall@10				
	MR	SVGA	ITR	FP	ARB		MR	SVGA	ITR	FP	ARB
40%	0.1876	0.1771	0.1675	0.1953		40%	0.1041	0.1059	0.1021	0.1184	
50%	0.1804	0.1737	0.1632	0.1893		50%	0.0996	0.1016	0.0933	0.1094	
60%	0.1718	0.1656	0.1620	0.1856		60%	0.0943	0.0972	0.0850	0.1046	
70%	0.1650	0.1546	0.1607	0.1781		70%	0.0846	0.0863	0.0830	0.0983	
80%	0.1586	0.1425	0.1582	0.1681		80%	0.0742	0.0740	0.0821	0.0897	
90%	0.1376	0.1102	0.1487	0.1602		90%	0.0607	0.0589	0.0623	0.0844	
99%	0.1121	0.0987	0.1420	0.1534		99%	0.0425	0.0423	0.0530	0.0765	
Avg.	0.1590	0.1461	0.1574	0.1757		Avg.	0.0800	0.0809	0.0801	0.0973	

Computers	Recall@10					Photo	Recall@10				
	MR	SVGA	ITR	FP	ARB		MR	SVGA	ITR	FP	ARB
40%	0.0430	0.0430	0.0435	0.0459		40%	0.0440	0.0428	0.0442	0.0465	
50%	0.0430	0.0429	0.0430	0.0458		50%	0.0440	0.0425	0.0441	0.0459	
60%	0.0437	0.0446	0.0425	0.0449		60%	0.0446	0.0434	0.0434	0.0455	
70%	0.0412	0.0420	0.0425	0.0446		70%	0.0433	0.0425	0.0432	0.0447	
80%	0.0410	0.0408	0.0429	0.0450		80%	0.0427	0.0416	0.0430	0.0445	
90%	0.0369	0.0377	0.0418	0.0434		90%	0.0394	0.0382	0.0423	0.0437	
99%	0.0284	0.0264	0.0410	0.0420		99%	0.0268	0.0278	0.0412	0.0434	
Avg.	0.0415	0.0396	0.0427	0.0449		Avg.	0.0430	0.0418	0.0434	0.0451	

G. Training Time Comparison Verification (Q6)

Since propagation methods do not require gradient descent operations, they naturally have an advantage over deep generative methods. Figure 7 shows that, under the same hardware conditions (NVIDIA GeForce RTX 3090 24G) and with SVGA’s loss converged, as well as 20 propagation iterations for both PCFI and ARB, ARB significantly outperforms the baseline methods SVGA (deep learning method) and PCFI (propagation method) in terms of training speed. Specifically, ARB is approximately **163** times faster than SVGA and **4.4** times faster than PCFI on average.

For propagation methods, Table X is conducted with the same number of propagation iterations $l = 20$. It can be observed that our ARB method incurs almost no additional runtime compared to FP. However, PCFI is approximately four times slower than FP. This is primarily because PCFI introduces confidence calculation, which involves searching neighborhood distances and computing the correlation matrix, thereby increasing computational complexity. Additionally, this method exceeded memory capacity on the Ogbn-Products dataset, forcing it to switch to CPU computation, which limited its scalability on large graphs. Overall, the analysis indicates that while ARB has computational efficiency comparable to FP, it significantly outperforms FP in terms of reconstruction accuracy.

Thus, in response to Q6, our conclusion is: **ARB is highly computationally efficient and low in complexity, making it well-suited for scaling to large graphs.**

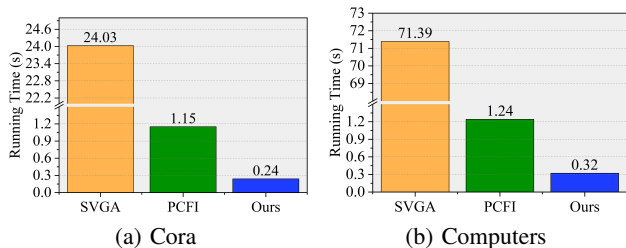


Fig. 7: Comparison of running time.

TABLE X: Comparison of running time (s). Best improvement is **blue**.

Method	Cora	CiteSeer	PubMed	Computers
FP	0.2327	0.2653	0.2434	0.3152
PCFI	1.1521($\times 4.95$)	1.2196($\times 4.60$)	1.2136($\times 4.99$)	1.2383($\times 3.93$)
Ours	0.2351($\times 1.01$)	0.2654($\times 1.01$)	0.2549($\times 1.05$)	0.3160($\times 1.01$)
Method	Photo	CS	Ogbn-Arxiv	Ogbn-Products
FP	0.2548	0.8377	0.3659	16.2063
PCFI	1.1614($\times 4.56$)	2.1147($\times 2.52$)	1.3760($\times 3.76$)	OOM.
Ours	0.2560($\times 1.01$)	0.8850($\times 1.06$)	0.3700($\times 1.01$)	16.5091($\times 1.02$)

VI. CONCLUSION

This paper presents *AttriReBoost* (ARB), a novel method for reconstructing missing attributes in graph data through

a propagation-based approach. ARB introduces two key innovations: redefining boundary conditions and incorporating virtual edges, which are specifically designed to address the cold start problem in attribute-missing graphs. The method operates without relying on gradient-based learning, offering a simplified and computationally efficient solution. Theoretical analysis rigorously proves ARB’s convergence, and empirical evaluations demonstrate its superior performance in attribute reconstruction and downstream node classification, with a notable reduction in training time. ARB’s efficiency and scalability position it as a competitive solution in the field of graph-based learning.

Future research will focus on three main directions. First, we will explore the relationship between missing attributes and propagation dynamics, aiming to understand how attribute sparsity impacts information flow and design more robust propagation mechanisms. Second, we will investigate alternative methods for constructing virtual edges, such as using graph generative models, structural similarities, or domain-specific heuristics. Finally, we plan to integrate ARB with GNNs as a pre-filling processor, developing adaptive mechanisms to handle varying levels of attribute incompleteness and diverse graph structures, expanding ARB’s applicability to a wider range of real-world scenarios.

REFERENCES

- [1] C. Ji, H. Chen, R. Wang, Y. Cai, and H. Wu, “Smoothness sensor: Adaptive smoothness-transition graph convolutions for attributed graph clustering,” *IEEE Transactions on Cybernetics*, vol. 52, no. 12, pp. 12 771–12 784, 2022.
- [2] S. Kuang, Y. Liu, X. Wang, X. Wu, and Y. Wei, “Harnessing multimodal large language models for traffic knowledge graph generation and decision-making,” *Communications in Transportation Research*, vol. 4, p. 100146, 2024.
- [3] M. Li, Y. Zhang, S. Wang, Y. Hu, and B. Yin, “Redundancy is not what you need: An embedding fusion graph auto-encoder for self-supervised graph representation learning,” *IEEE Transactions on Neural Networks and Learning Systems*, 2024.
- [4] R. Yuan, Y. Tang, Y. Wu, J. Niu, and W. Zhang, “Semi-supervised graph structure learning via dual reinforcement of label and prior structure,” *IEEE Transactions on Cybernetics*, vol. 54, no. 11, pp. 6943–6956, 2024.
- [5] Z. Liu, C. Li, Y. Wang, N. Yang, X. Fan, J. Ma, and X. Zhao, “Multi-scale temporal fusion transformer for incomplete vehicle trajectory prediction,” *arXiv preprint arXiv:2409.00904*, 2024.
- [6] Z. Peng, W. Huang, M. Luo, Q. Zheng, Y. Rong, T. Xu, and J. Huang, “Graph representation learning via graphical mutual information maximization,” in *Proceedings of The Web Conference*, 2020, pp. 259–270.
- [7] D. Adhikari, W. Jiang, J. Zhan, Z. He, D. B. Rawat, U. Aickelin, and H. A. Khorshidi, “A comprehensive survey on imputation of missing data in internet of things,” *ACM Computing Surveys*, vol. 55, no. 7, pp. 1–38, 2022.
- [8] C. Gao, J. Zhu, F. Zhang, Z. Wang, and X. Li, “A novel representation learning for dynamic graphs based on graph convolutional networks,” *IEEE Transactions on Cybernetics*, vol. 53, no. 6, pp. 3599–3612, 2023.
- [9] M. Li, R. Zhang, Y. Zhang, X. Piao, S. Zhao, and B. Yin, “Scae: Structural contrastive auto-encoder for incomplete multi-view representation learning,” *ACM Transactions on Multimedia Computing, Communications and Applications*, vol. 20, no. 9, pp. 1–24, 2024.
- [10] J. You, X. Ma, D. Y. Ding, M. Kochenderfer, and J. Leskovec, “Handling missing data with graph representation learning,” in *Proceedings of the International Conference on Neural Information Processing Systems*, 2020, pp. 19 075–19 087.
- [11] D. Guo, Z. Chu, and S. Li, “Fair attribute completion on graph with missing attributes,” *arXiv preprint arXiv:2302.12977*, 2023.
- [12] X. Chen, S. Chen, J. Yao, H. Zheng, Y. Zhang, and I. W. Tsang, “Learning on attribute-missing graphs,” *IEEE Transactions on Pattern Analysis and Machine Intelligence*, vol. 44, no. 2, pp. 740–757, 2022.

- [13] J. Yoo, H. Jeon, J. Jung, and U. Kang, "Accurate node feature estimation with structured variational graph autoencoder," in *Proceedings of the ACM SIGKDD Conference on Knowledge Discovery and Data Mining*, 2022, pp. 2336–2346.
- [14] W. Tu, S. Zhou, X. Liu, Y. Liu, Z. Cai, E. Zhu, Z. Changwang, and J. Cheng, "Initializing then refining: A simple graph attribute imputation network," in *Proceedings of the AAAI International Conference on Artificial Intelligence*, 2022, pp. 3494–3500.
- [15] D. Chen, Y. Lin, W. Li, P. Li, J. Zhou, and X. Sun, "Measuring and relieving the over-smoothing problem for graph neural networks from the topological view," in *Proceedings of the AAAI Conference on Artificial Intelligence*, vol. 34, no. 04, 2020, pp. 3438–3445.
- [16] E. Rossi, H. Kenlay, M. I. Gorinova, B. P. Chamberlain, X. Dong, and M. M. Bronstein, "On the unreasonable effectiveness of feature propagation in learning on graphs with missing node features," in *Learning on Graphs Conference*. PMLR, 2022, pp. 11–1.
- [17] D. Um, J. Park, S. Park, and J. Y. Choi, "Confidence-based feature imputation for graphs with partially known features," *arXiv preprint arXiv:2305.16618*, 2023.
- [18] W. Zheng, E. W. Huang, N. Rao, S. Katariya, Z. Wang, and K. Subbian, "Cold brew: Distilling graph node representations with incomplete or missing neighborhoods," *arXiv preprint arXiv:2111.04840*, 2021.
- [19] Z. Zhou, Y. Hu, Y. Zhang, J. Chen, and H. Cai, "Multiview deep graph infomax to achieve unsupervised graph embedding," *IEEE Transactions on Cybernetics*, vol. 53, no. 10, pp. 6329–6339, 2023.
- [20] J. Gasteiger, A. Bojchevski, and S. Günnemann, "Predict then propagate: Graph neural networks meet personalized pagerank," *arXiv preprint arXiv:1810.05997*, 2018.
- [21] H. Robbins and S. Monro, "A Stochastic Approximation Method," *The Annals of Mathematical Statistics*, vol. 22, no. 3, pp. 400–407, 1951.
- [22] Ö. Şimşek and D. Jensen, "Navigating networks by using homophily and degree," *Proceedings of the National Academy of Sciences*, vol. 105, no. 35, pp. 12 758–12 762, 2008.
- [23] J.-F. Cai, E. J. Candès, and Z. Shen, "A singular value thresholding algorithm for matrix completion," *SIAM Journal on Optimization*, vol. 20, no. 4, pp. 1956–1982, 2010.
- [24] J. Wen, Y. Xu, and H. Liu, "Incomplete multiview spectral clustering with adaptive graph learning," *IEEE Transactions on Cybernetics*, vol. 50, no. 4, pp. 1418–1429, 2020.
- [25] J. Wen, Z. Zhang, Z. Zhang, L. Fei, and M. Wang, "Generalized incomplete multiview clustering with flexible locality structure diffusion," *IEEE Transactions on Cybernetics*, vol. 51, no. 1, pp. 101–114, 2021.
- [26] W. Xia, Q. Gao, Q. Wang, and X. Gao, "Tensor completion-based incomplete multiview clustering," *IEEE Transactions on Cybernetics*, vol. 52, no. 12, pp. 13 635–13 644, 2022.
- [27] S. Yu, P. Zhang, S. Wang, Z. Dong, H. Yang, E. Zhu, and X. Liu, "Differentiated anchor quantity assisted incomplete multiview clustering without number-tuning," *IEEE Transactions on Cybernetics*, vol. 54, no. 11, pp. 7024–7037, 2024.
- [28] J. Yoon, J. Jordon, and M. Schaar, "Gain: Missing data imputation using generative adversarial nets," in *Proceedings of the International Conference on Machine Learning*. PMLR, 2018, pp. 5689–5698.
- [29] X. Huang, Q. Song, Y. Li, and X. Hu, "Graph recurrent networks with attributed random walks," in *Proceedings of the ACM SIGKDD International Conference on Knowledge Discovery & Data Mining*, 2019, pp. 732–740.
- [30] L. Chen, J. Bruna, and M. Bronstein, "Attributed random walk as matrix factorization," in *Proceedings of the International Conference on Neural Information Processing Systems, Graph Representation Learning Workshop*, 2019.
- [31] I. Spinelli, S. Scardapane, and A. Uncini, "Missing data imputation with adversarially-trained graph convolutional networks," *Neural Networks*, vol. 129, pp. 249–260, 2020.
- [32] H. Taguchi, X. Liu, and T. Murata, "Graph convolutional networks for graphs containing missing features," *Future Generation Computer Systems*, vol. 117, pp. 155–168, 2021.
- [33] T. N. Kipf and M. Welling, "Semi-supervised classification with graph convolutional networks," *arXiv preprint arXiv:1609.02907*, 2016.
- [34] S. L. Lauritzen and D. J. Spiegelhalter, "Local computations with probabilities on graphical structures and their application to expert systems," *Journal of the Royal Statistical Society: Series B (Methodological)*, vol. 50, no. 2, pp. 157–194, 1988.
- [35] D. Jin, R. Wang, T. Wang, D. He, W. Ding, Y. Huang, L. Wang, and W. Pedrycz, "Amer: A new attribute-missing network embedding approach," *IEEE Transactions on Cybernetics*, vol. 53, no. 7, pp. 4306–4319, 2022.
- [36] Z. Gao, Y. Niu, J. Cheng, J. Tang, L. Li, T. Xu, P. Zhao, F. Tsung, and J. Li, "Handling missing data via max-entropy regularized graph autoencoder," in *Proceedings of the AAAI Conference on Artificial Intelligence*, vol. 37, no. 6, 2023, pp. 7651–7659.
- [37] M. Li, Y. Zhang, W. Zhang, S. Zhao, X. Piao, and B. Yin, "Csat: Contrastive sampling-aggregating transformer for community detection in attribute-missing networks," *IEEE Transactions on Computational Social Systems*, vol. 11, no. 2, pp. 2277–2290, 2024.
- [38] X. Peng, J. Cheng, X. Tang, B. Zhang, and W. Tu, "Multi-view graph imputation network," *Information Fusion*, vol. 102, p. 102024, 2024.
- [39] B. Hao, J. Zhang, H. Yin, C. Li, and H. Chen, "Pre-training graph neural networks for cold-start users and items representation," in *Proceedings of the ACM International Conference on Web Search and Data Mining*, 2021, pp. 265–273.
- [40] Y. Gong, X. Ding, Y. Su, K. Shen, Z. Liu, and G. Zhang, "An unified search and recommendation foundation model for cold-start scenario," in *Proceedings of the ACM International Conference on Information and Knowledge Management*, 2023, pp. 4595–4601.
- [41] D. Cai, S. Qian, Q. Fang, J. Hu, and C. Xu, "User cold-start recommendation via inductive heterogeneous graph neural network," *ACM Transactions on Information Systems*, vol. 41, no. 3, pp. 1–27, 2023.
- [42] C. Yang, J. Liu, and C. Shi, "Extract the knowledge of graph neural networks and go beyond it: An effective knowledge distillation framework," in *Proceedings of the Web Conference*, 2021, pp. 1227–1237.
- [43] F. Huang, Z. Wang, X. Huang, Y. Qian, Z. Li, and H. Chen, "Aligning distillation for cold-start item recommendation," in *Proceedings of the International ACM SIGIR Conference on Research and Development in Information Retrieval*, 2023, pp. 1147–1157.
- [44] G. Aubert and L. Vese, "A variational method in image recovery," *SIAM Journal on Numerical Analysis*, vol. 34, no. 5, pp. 1948–1979, 1997.
- [45] S. Loncaric, "A survey of shape analysis techniques," *Pattern Recognition*, vol. 31, no. 8, pp. 983–1001, 1998.
- [46] F. R. Chung, *Spectral graph theory*. American Mathematical Soc., 1997, vol. 92.
- [47] S. Banach, "Sur les opérations dans les ensembles abstraits et leur application aux équations intégrales," *Fundamenta Mathematicae*, vol. 3, no. 1, pp. 133–181, 1922.
- [48] P. Veličković, G. Cucurull, A. Casanova, A. Romero, P. Lio, and Y. Bengio, "Graph attention networks," *arXiv preprint arXiv:1710.10903*, 2017.
- [49] F. Wu, A. Souza, T. Zhang, C. Fifty, T. Yu, and K. Weinberger, "Simplifying graph convolutional networks," in *Proceedings of the Conference on International Conference on Machine Learning*. PMLR, 2019, pp. 6861–6871.
- [50] Z. Yang, W. Cohen, and R. Salakhudinov, "Revisiting semi-supervised learning with graph embeddings," in *Proceedings of the International Conference on Machine Learning*. PMLR, 2016, pp. 40–48.
- [51] O. Shchur, M. Mumme, A. Bojchevski, and S. Günnemann, "Pitfalls of graph neural network evaluation," *arXiv preprint arXiv:1811.05868*, 2018.
- [52] W. Hu, M. Fey, M. Zitnik, Y. Dong, H. Ren, B. Liu, M. Catasta, and J. Leskovec, "Open graph benchmark: Datasets for machine learning on graphs," *Proceedings of the Conference in Neural Information Processing Systems*, vol. 33, pp. 22 118–22 133, 2020.
- [53] W. L. Hamilton, R. Ying, and J. Leskovec, "Inductive representation learning on large graphs," in *Proceedings of the International Conference on Neural Information Processing Systems*, 2017, pp. 1025–1035.



Mengran Li is currently pursuing a Ph.D. degree at the Guangdong Key Laboratory of Intelligent Transportation Systems, School of Intelligent Systems Engineering, Sun Yat-sen University, Shenzhen, P.R. China. He received an M.S. degree in Control Science and Engineering from the Beijing Key Laboratory of Multimedia and Intelligent Software Technology, Beijing University of Technology, Beijing, P.R. China, in 2023. His research interests include graph neural networks, data mining, and complex network optimization.



Chaojun Ding is currently working as a Research Assistant at the Guangdong Key Laboratory of Intelligent Transportation Systems, School of Intelligent Systems Engineering, Shenzhen Campus of Sun Yat-sen University, Shenzhen, P.R. China. She received her master's degree in Applied Mathematics from P.R. China University of Geosciences. Her research interests include data mining and distributed graph computing.



Junzhou Chen received his Ph.D. in Computer Science and Engineering from the Chinese University of Hong Kong in 2008. Between March 2009 and February 2019, he served as a Lecturer and later as an Associate Professor at the School of Information Science and Technology at Southwest Jiaotong University. He is currently an Associate Professor at School of Intelligent Systems Engineering at Shenzhen Campus of Sun Yat-sen University. His research interests include computer vision, machine learning and intelligent transportation systems.



Wenbin Xing received his B.S. degree in Computer Science and Technology from Wuhan University of Technology, Wuhan, P.R. China, in 2024. He is pursuing his master's degree at Sun Yat-sen University in Shenzhen, P.R. China. His current research interests include autonomous driving, traffic big data, deep learning, and spatial-temporal modeling.



Cong Ye received the B.Sc. degree in vehicle engineering from Hefei University of Technology, Hefei, P.R. China, in 2020, and the M.S. degree in vehicle engineering from Jilin University, Changchun, P.R. China, in 2023. He is currently working toward the Ph.D. degree in Electronic Information at the School of Intelligent Engineering, Sun Yat-sen University in Shenzhen, P.R. China. His research interests include vehicle dynamics, x-by-wire chassis, and autonomous driving.



Ronghui Zhang received a B.Sc. (Eng.) from the Department of Automation Science and Electrical Engineering, Hebei University, Baoding, P.R. China, in 2003, an M.S. degree in Vehicle Application Engineering from Jilin University, Changchun, P.R. China, in 2006, and a Ph.D. (Eng.) in Mechanical & Electrical Engineering from Changchun Institute of Optics, Fine Mechanics and Physics, the Chinese Academy of Sciences, Changchun, P.R. China, in 2009. After finishing his post-doctoral research work at INRIA, Paris, France, in February 2011, he is currently an Associate Professor with Guangdong Key Laboratory of Intelligent Transportation System, School of Intelligent Systems Engineering, Shenzhen Campus of Sun Yat-sen University, Shenzhen, Guangdong, P.R. China. His current research interests include computer vision, intelligent control, and ITS.



Songlin Zhuang received the B.E. degree in automation and the Ph.D. degree in control science and engineering from the Harbin Institute of Technology, Harbin, P.R. China, in 2014 and 2019, respectively. From 2019 to 2020, he was a Postdoctoral Fellow with the Department of Mechanical and Industrial Engineering, University of Toronto, Toronto, Canada. From 2020 to 2023, he was a Postdoctoral Fellow with the Department of Mechanical Engineering, University of Victoria, Victoria, Canada. He is currently a Professor with Yongjiang Laboratory, Ningbo, P.R. China. His research interests include micro/nano-manipulation and control theory. He serves as a Technical Editor of IEEE/ASME Transactions on Mechatronics.



Jia Hu works as a ZhongTe Distinguished Chair in Cooperative Automation in the College of Transportation Engineering at Tongji University. Before joining Tongji, he was a research associate at the Federal Highway Administration, USA (FHWA). He serves as an associate editor for IEEE Trans. Intell. Transp. Syst., IEEE Trans. Intell. Veh., ASCE J. Transp. Eng., and IEEE Open J. Intell. Transp. Syst.. He is also an assistant editor of the J. Intell. Transp. Syst., an advisory editorial board member for Transp. Res. Part C, an associate editor for the IEEE Intell. Veh. Symp. since 2018, and an associate editor for the IEEE Intell. Transp. Syst. Conf. since 2019.



Tony Z. Qiu is a Professor in the Faculty of Engineering at the University of Alberta, Canada Research Chair Professor in Cooperative Transportation Systems, and Director of the Centre for Smart Transportation. Dr. Tony Qiu received his PhD degree from the University of Wisconsin-Madison, and worked as a Post-Doctoral Researcher in the California PATH Program at the University of California, Berkeley, before joining the University of Alberta. Dr. Tony Qiu has been awarded the Minister's Award of Excellence in 2013, the Faculty of Engineering Annual Research Award in 2015-2016, and the ITS Canada Annual Innovation and R&D Award in 2016 and 2017. His research interest includes traffic operation and control, traffic flow theory, and traffic model analytics. He has published more than 180 papers in international journals and academic conferences, and has 7 awarded patents and 5 pending application patents.



Huijun Gao (Fellow, IEEE) received the Ph.D. degree in control science and engineering from the Harbin Institute of Technology, Harbin, P.R. China, in 2005. Since 2004, he has been with the Harbin Institute of Technology, where he is currently the Chair Professor and the Director of the Research Institute of Intelligent Control and Systems. From 2005 to 2007, he carried out his post-doctoral research with the Department of Electrical and Computer Engineering, University of Alberta, Edmonton, AB, Canada. His research interests include intelligent and robust control, robotics, mechatronics, and their engineering applications. Dr. Gao is a member of Academia Europaea and the Vice President of the IEEE Industrial Electronics Society. He was a recipient of the 2022 Dr.-Ing. Eugene Mittelmann Achievement Award and the 2023 Norbert Wiener Award. He is a Distinguished Lecturer of the IEEE Systems, Man and Cybernetics Society. He is/was the Editor-in-Chief of IEEE/ASME Transactions on Mechatronics, the Co-Editor-in-Chief of IEEE Transactions on Industrial Electronics, and an Associate Editor of Automatica, IEEE Transactions on Cybernetics, and IEEE Transactions on Industrial Informatics.

SUPPLEMENTARY APPENDIX

A. Proof of New Boundary Conditions

Statement 1: presents the optimization loss for Redefinition of Boundary Conditions to dynamically adjust the initialization of known nodes.

Define:

$$\mathbf{I}_k^0 = \text{diag}(\{\lambda_1, \lambda_2, \dots, \lambda_N\}), \lambda_i = \begin{cases} 1 & \text{if } i \in \mathcal{V}_k \\ 0 & \text{otherwise} \end{cases} \quad (15)$$

$$\mathbf{I}_u^0 = \text{diag}(\{\lambda_1, \lambda_2, \dots, \lambda_N\}), \tilde{\lambda}_i = \begin{cases} 0 & \text{if } i \in \mathcal{V}_k \\ 1 & \text{otherwise} \end{cases} \quad (16)$$

Then:

$$\begin{aligned} \nabla \mathcal{L}(\mathbf{X}) &= \mathbf{L}\mathbf{X} + \eta(\mathbf{X}_k - \mathbf{Z}_k) = 0 \\ \implies \mathbf{L}\mathbf{X} + \eta\mathbf{I}_k^0(\mathbf{X} - \mathbf{Z}) &= 0 \\ \implies (\mathbf{I} + \eta\mathbf{I}_k^0)\mathbf{X} &= \tilde{\mathbf{A}}\mathbf{X} + \eta\mathbf{I}_k^0\mathbf{Z} \\ \implies ((1 + \eta)\mathbf{I}_k^0 + \mathbf{I}_u^0)\mathbf{X} &= \tilde{\mathbf{A}}\mathbf{X} + \eta\mathbf{I}_k^0\mathbf{Z} \\ \implies \mathbf{X} &= \left(\frac{1}{1 + \eta}\mathbf{I}_k^0 + \mathbf{I}_u^0\right)(\tilde{\mathbf{A}}\mathbf{X} + \eta\mathbf{I}_k^0\mathbf{Z}) \\ \implies \mathbf{X} &= \mathbf{I}_u^0\tilde{\mathbf{A}}\mathbf{X} + \mathbf{I}_k^0\left(\frac{1}{1 + \eta}\tilde{\mathbf{A}}\mathbf{X} + \frac{\eta}{1 + \eta}\mathbf{Z}\right) \\ \implies \mathbf{X} &= \mathbf{I}_u^0\tilde{\mathbf{A}}\mathbf{X} + \mathbf{I}_k^0(\beta\tilde{\mathbf{A}}\mathbf{X} + (1 - \beta)\mathbf{Z}) \\ \implies \begin{bmatrix} \mathbf{X}_k \\ \mathbf{X}_u \end{bmatrix} &= \begin{bmatrix} \beta(\tilde{\mathbf{A}}\mathbf{X})_k + (1 - \beta)\mathbf{Z}_k \\ (\tilde{\mathbf{A}}\mathbf{X})_u \end{bmatrix} \\ \implies \mathbf{X} &= \beta\tilde{\mathbf{A}}\mathbf{X} + (1 - \beta)\begin{bmatrix} \mathbf{Z}_k \\ (\tilde{\mathbf{A}}\mathbf{X})_u \end{bmatrix} \end{aligned} \quad (17)$$

So:

$$\begin{cases} \mathbf{X} = \tilde{\mathbf{A}}\mathbf{X}, \\ \mathbf{X}_k = \beta\mathbf{X}_k + (1 - \beta)\mathbf{Z}_k \end{cases} \quad (18)$$

□ *Convergence Proof*

The Equation (18) can be written as:

$$\begin{bmatrix} \mathbf{X}_k \\ \mathbf{X}_u \end{bmatrix} = \begin{bmatrix} \beta\mathbf{A}_{kk} & \beta\mathbf{A}_{ku} \\ \mathbf{A}_{uk} & \mathbf{A}_{uu} \end{bmatrix} \begin{bmatrix} \mathbf{X}_k \\ \mathbf{X}_u \end{bmatrix} + \begin{bmatrix} (1 - \beta)\mathbf{Z}_k \\ 0 \end{bmatrix} \quad (19)$$

Let

$$\mathbf{K} = \begin{bmatrix} \beta\mathbf{A}_{kk} & \beta\mathbf{A}_{ku} \\ \mathbf{A}_{uk} & \mathbf{A}_{uu} \end{bmatrix}, \quad \mathbf{C} = \begin{bmatrix} (1 - \beta)\mathbf{Z}_k \\ 0 \end{bmatrix} \quad (20)$$

Here $\beta \in [0, 1)$, then $0 \leq \mathbf{K} \leq \tilde{\mathbf{A}}$ elementwise and $\mathbf{K} \neq \tilde{\mathbf{A}}$. According to Section III D in this paper, $\rho(\mathbf{K}) < 1$, Equation (23) converges. This completes the proof. ■

B. Proof of Virtual Edges

Statement 1: presents the optimization loss for Virtual Edges, to ensure robust connectivity in the attribute-missing graph.

Define:

$$\mathbf{I}_k^0 = \text{diag}(\{\lambda_1, \lambda_2, \dots, \lambda_N\}), \lambda_i = \begin{cases} 1 & \text{if } i \in \mathcal{V}_k \\ 0 & \text{otherwise} \end{cases} \quad (21)$$

Then:

$$\begin{aligned} \nabla \mathcal{L}(\mathbf{X}) &= 0 \\ \implies \mathbf{I}_k^0(\mathbf{L}\mathbf{X} + \theta\mathbf{L}_1\mathbf{X}) &= 0 \\ \implies \mathbf{I}_k^0 \left[(1 + \theta)\mathbf{X} - (\tilde{\mathbf{A}} + \theta\tilde{\mathbf{A}}_1)\mathbf{X} \right] &= 0 \\ \implies \mathbf{I}_k^0 \left[(1 + \theta)\mathbf{X} - \tilde{\mathbf{A}}\mathbf{X} - \theta\left(\frac{1}{N-1}\mathbf{J}_{N \times N} - \frac{1}{N-1}\mathbf{I}\right)\mathbf{X} \right] &= 0 \\ \implies \mathbf{I}_k^0 \left[(1 + \theta)\mathbf{X} - \tilde{\mathbf{A}}\mathbf{X} - \theta\left(\frac{N}{N-1}\bar{\mathbf{X}} - \frac{1}{N-1}\mathbf{X}\right) \right] &= 0 \\ \implies \mathbf{I}_k^0 \left[\left(1 + \theta + \frac{\theta}{N-1}\right)\mathbf{X} - (\tilde{\mathbf{A}}\mathbf{X} + \theta\frac{N}{N-1}\bar{\mathbf{X}}) \right] &= 0 \\ \implies \mathbf{I}_k^0 \left[\mathbf{X} - \frac{N-1}{N + \theta N - 1}\tilde{\mathbf{A}}\mathbf{X} - \frac{\theta N}{N + \theta N - 1}\bar{\mathbf{X}} \right] &= 0 \\ \implies \mathbf{I}_k^0 \left[\mathbf{X} - \alpha\tilde{\mathbf{A}}\mathbf{X} - (1 - \alpha)\bar{\mathbf{X}} \right] &= 0 \end{aligned} \quad (22)$$

So:

$$\begin{cases} \mathbf{X} = \alpha\tilde{\mathbf{A}}\mathbf{X} + (1 - \alpha)\bar{\mathbf{X}} \\ \mathbf{X}_k = \mathbf{Z}_k \end{cases} \quad (23)$$

□ *Convergence Proof*

Let:

$$\mathbf{B} = \alpha\tilde{\mathbf{A}} + (1 - \alpha)\frac{1}{N}\mathbf{J} \quad (24)$$

where \mathbf{J} is an all-ones matrix, $\rho(\frac{1}{N}\mathbf{J}) = 1$. So \mathbf{B} is a strongly connected matrix. According to $\rho(\tilde{\mathbf{A}}) \leq 1$, $\rho(\mathbf{B}) \leq 1$. Equation (23) can be written as:

$$\mathbf{X} = \begin{bmatrix} 0 & 0 \\ \mathbf{B}_{uk} & \mathbf{B}_{uu} \end{bmatrix} \mathbf{X} + \begin{bmatrix} \mathbf{Z}_k \\ 0 \end{bmatrix} \quad (25)$$

Let:

$$\mathbf{K} = \begin{bmatrix} 0 & 0 \\ \mathbf{B}_{uk} & \mathbf{B}_{uu} \end{bmatrix}, \quad \mathbf{C} = \begin{bmatrix} \mathbf{Z}_k \\ 0 \end{bmatrix} \quad (26)$$

Then $0 \leq \mathbf{K} \leq \mathbf{B}$ elementwise and $\mathbf{K} \neq \mathbf{B}$. According to Section III D in this paper, $\rho(\mathbf{K}) < 1$, Equation (23) converges. This completes the proof. ■

From the above proofs, our ARB can be simplified into two forms, represented by Equations (23) and (18), each tailored to different graph structures. The hyperparameters α and β are not set based on intuition but are derived through the optimization equation. Moreover, when both are set to 1, ARB degenerates into FP.